

## Hamiltonian tomography of photonic lattices

Ruichao Ma, Clai Owens, Aman LaChapelle, David I. Schuster, and Jonathan Simon

*James Franck Institute and Department of Physics at University of Chicago, Chicago, Illinois 60637, USA*

(Received 8 April 2017; published 26 June 2017)

In this paper we introduce an approach to Hamiltonian tomography of noninteracting tight-binding photonic lattices. To begin with, we prove that the matrix element of the low-energy effective Hamiltonian between sites  $\alpha$  and  $\beta$  may be obtained directly from  $S_{\alpha\beta}(\omega)$ , the (suitably normalized) two-port measurement between sites  $\alpha$  and  $\beta$  at frequency  $\omega$ . This general result enables complete characterization of both on-site energies and tunneling matrix elements in arbitrary lattice networks by spectroscopy, and suggests that coupling between lattice sites is a topological property of the two-port spectrum. We further provide extensions of this technique for measurement of band projectors in finite, disordered systems with good band flatness ratios, and apply the tool to direct real-space measurement of the Chern number. Our approach demonstrates the extraordinary potential of microwave quantum circuits for exploration of exotic synthetic materials, providing a clear path to characterization and control of single-particle properties of Jaynes-Cummings-Hubbard lattices. More broadly, we provide a robust, unified method of spectroscopic characterization of linear networks from photonic crystals to microwave lattices and everything in between.

DOI: [10.1103/PhysRevA.95.062120](https://doi.org/10.1103/PhysRevA.95.062120)

### I. INTRODUCTION

The curse and blessing of synthetic quantum materials is the control these systems afford. This control enables access to near-arbitrary lattice geometries [1–4], tunable interaction range [5], and all variety of state and phase preparation and readout techniques [6–8]. The challenge is that every added degree of control provides another opportunity for disorder to creep in, substantially altering the anticipated many-body physics. A variety of approaches have been developed to control disorder, ranging from projection of corrective potentials onto cold atoms [9] to improving lattice fabrication in superconducting circuits [10] and 2DEGs [11]. Indeed, as fabrication techniques have improved in 2DEGs, the accessible fractional Hall landscape has opened for study of immense array of exciting topological phases, and it seems other synthetic material systems could follow a similar trend.

If disorder is to be corrected site by site, it must be characterized locally. This task is challenging, because information about the on-site energy of a lattice site and its tunneling rates to its neighbors are encoded nontrivially and nonlocally in the eigenvalue and eigenvector spectrum of the system. In the case of a 1D tight-binding chain, the reflection spectrum off of the system end is sufficient to extract the full noninteracting Hamiltonian (see [12] and Appendix B). For a 2D lattice of known topology, it is possible to make measurements along a 1D boundary to extract the Hamiltonian parameters [13], with sufficiently high signal to noise. Here we point out a unique opportunity to employ direct spectroscopic tools to extract particular desired matrix elements of the single-particle Hamiltonian. Building on prior theoretical work connecting sum rules to linear response measurements [14], we describe a general technique for resolving matrix elements of an arbitrarily connected Hamiltonian between lattice sites via simple two-port transmission and one-port reflection (local density of states) measurements. We then extend the technique to robust measurement of band projectors and Chern numbers, supplementing prior works that rely on physically modifying the lattice structure [15,16], or dissipation-calibrated measures of transverse displacement [17].

### II. THEORY OF LATTICE SPECTROSCOPY

#### A. Formulas for arbitrary linear networks

Suppose that we would like to characterize a noninteracting network of lattice sites in the site basis, by answering specific questions like “what is the energy cost to put a particle on site  $\alpha$ ?” or “what is the tunnel-coupling between sites  $\alpha$  and  $\beta$ ?” One might attempt to characterize the full lattice by performing two-port measurements between all pairs of sites  $(m,n)$ , and then fitting the results with an analytic model to extract the underlying lattice parameters. This works in principle, but generally is highly susceptible to noise and requires  $O(N^2)$  measurements (except in the 1D case; see Appendix B); here we prove that the information for matrix elements of the Hamiltonian  $H_{\alpha\beta}$  is entirely encoded in the frequency-dependent two-port measurement  $S_{\alpha\beta}(\omega)$  between only the two sites  $\alpha$  and  $\beta$  of interest, by connecting experimentally measurable quantities in linear photonic lattices to theoretical results for sum rules of response functions [14].

Let the system Hamiltonian be given by (in what follows we set  $\hbar = 1$ )

$$H = \sum_l (\omega_l + i\kappa_l/2) a_l^\dagger a_l - \sum_{\alpha \neq \beta} t_{\alpha\beta} a_\alpha^\dagger a_\beta, \quad (1)$$

where  $a_\alpha^\dagger (a_\alpha)$  creates (destroys) a photon on site  $\alpha$ ,  $t_{\alpha\beta}$  is the direct tunnel coupling between sites  $\alpha$  and  $\beta$ ,  $\omega_l$  is the energy cost to place a photon on site  $l$ , and  $\kappa_l$  is the linewidth of a photon on site  $l$  including contributions from both internal loss and loss from out coupling. We have employed a non-Hermitian Hamiltonian formalism which applies in the weak-driving limit [18–20]. In this limit, the resonator transmission ( $S$  matrix) between sites  $\alpha$  and  $\beta$  at frequency  $\omega$  is given by [21,22]

$$S_{\alpha\beta}^{\text{full}}(\omega) = \delta_{\alpha\beta} - i\sqrt{\kappa_\alpha^\alpha \kappa_\beta^\beta} \langle \alpha | \frac{1}{\omega - H} | \beta \rangle. \quad (2)$$

Here  $|l\rangle$  [for  $l \in (\alpha, \beta)$ ] is the quantum state with a single photon at site  $l$ :  $|l\rangle \equiv a_l^\dagger |0\rangle$ , where  $|0\rangle$  is the vacuum state. We have assumed that our physical system always has out coupling

at every site; the part of the resonator loss at site  $l$ ,  $\kappa_l$ , that arises due to out coupling rather than internal loss, is labeled  $\kappa_c^l$ . This quantity is entirely *real*—imaginary out coupling would be a shift of the resonance, and this effect is incorporated into the resonator frequency  $\omega_l$ . For the rest of this paper, we consider the offset-corrected  $S$  matrix  $S_{\alpha\beta} \equiv S_{\alpha\beta}^{\text{full}} - \delta_{\alpha\beta}$ , where the contribution from direct reflection has been subtracted.

Before proceeding, it is worthwhile to take a moment to outline the realm of validity of our approach. For a truly linear system such as the one described above, the drive strength may in fact be arbitrarily large, so long as  $S_{\alpha\beta}$  is reinterpreted as a two-point measurement of creation and annihilation operators, rather than single-photon states [23]. More generally, however, we aim to employ this method to quantify the linear properties of strongly nonlinear systems [24], in which case it is sufficient to require that the probe Rabi frequency be small compared with the smallest  $\kappa_i$  in the system: otherwise, the system will be populated with multiple excitations, and the linear Hamiltonian would no longer be sufficient. We furthermore assume that the manifolds with well-defined excitation numbers are isolated from one another: that is, there should be no accidental degeneracies between manifolds with  $n$  and  $m$  excitations, for  $n \neq m$ , as these could be mixed by a nonlinearity thereby breaking the approximations that give rise to a simple connection of Eq. (2) between the  $S$  matrix and the Hamiltonian.

With these considerations in mind, we examine  $\text{Pr}(\int \omega S_{\alpha\beta}(\omega) d\omega)$ , which diverges without the Cauchy principal value  $\text{Pr}()$ . To perform the integration, we employ the following definitions:  $|\mu\rangle$  is the single-photon eigenstate of  $H$  with eigenvalue  $\epsilon_\mu$ , and  $\langle v|$  is the element of the dual space to  $|\mu\rangle$  defined such that  $\langle v|\mu\rangle = \delta_{\mu\nu}$ ; note that  $\langle v| \neq [|\nu\rangle]^\dagger$ , because  $H$  is not Hermitian, so the matrix of eigenvectors is not unitary. We can then write

$$\begin{aligned}
& \int \omega S_{\alpha\beta}(\omega) d\omega \\
&= -i \int \omega \sqrt{\kappa_c^\alpha \kappa_c^\beta} \langle \alpha | \frac{1}{\omega - H} | \beta \rangle d\omega \\
&= -i \sqrt{\kappa_c^\alpha \kappa_c^\beta} \int \omega \langle \alpha | \sum_\mu \frac{|\mu\rangle \langle \mu|}{\omega - \epsilon_\mu} | \beta \rangle d\omega \\
&= -i \sqrt{\kappa_c^\alpha \kappa_c^\beta} \langle \alpha | \sum_\mu \left[ \int \omega \frac{|\mu\rangle \langle \mu|}{\omega - \epsilon_\mu} d\omega \right] | \beta \rangle \\
&= -i \sqrt{\kappa_c^\alpha \kappa_c^\beta} \langle \alpha | \sum_\mu \left[ \int \left( 1 + \frac{\epsilon_\mu}{\omega - \epsilon_\mu} \right) |\mu\rangle \langle \mu| d\omega \right] | \beta \rangle \\
&= -i \sqrt{\kappa_c^\alpha \kappa_c^\beta} \langle \alpha | \left[ W + i\pi \sum_\mu |\mu\rangle \epsilon_\mu \langle \mu| \right] | \beta \rangle \\
&= -i \sqrt{\kappa_c^\alpha \kappa_c^\beta} (W \langle \alpha | \beta \rangle + i\pi \langle \alpha | H | \beta \rangle). \tag{3}
\end{aligned}$$

Here  $W$  is the range of integration, and the sum only includes poles within this range. We have further assumed that the total bandwidth of the features under consideration is a small fraction of the center frequency, allowing us to assume the losses  $\kappa$  are frequency independent; more sophisticated techniques are required for truly broadband experiments [25,26], or for dissipation into structured continua. To extract

the coupling strengths  $\kappa_c^{\alpha,\beta}$ , we must also measure the one-port reflections  $S_{\alpha\alpha}(\omega)$  and  $S_{\beta\beta}(\omega)$ . An analogous calculation reveals that  $\int S_{\alpha\alpha}(\omega) d\omega = \pi \kappa_c^\alpha$  (see Appendix C), allowing us to write

$$\langle \alpha | H | \beta \rangle = \frac{\int \omega S_{\alpha\beta}(\omega) d\omega}{\sqrt{(\int S_{\alpha\alpha}(\omega) d\omega)(\int S_{\beta\beta}(\omega) d\omega)}} - \frac{W \langle \alpha | \beta \rangle}{i\pi}. \tag{4}$$

Thus we see that the matrix element of the Hamiltonian that couples a single photon in site  $\alpha$  to site  $\beta$  is given by the expectation of frequency weighted by the two-port measurement (as measured by a vector network analyzer, for example) between those two sites, properly normalized by one-port reflection measurements. If  $\alpha \neq \beta$ , then such a measurement provides the tunneling matrix element  $t_{\alpha\beta}$ , including its phase. If  $\alpha = \beta$ , this is an offset-subtracted reflection measurement, and it results in  $\omega_\alpha + i\kappa_\alpha/2$ , the on-site energy at site  $\alpha$ , with the imaginary part providing the on-site resonator linewidth. For sites which are not directly connected, the measurement will result in a zero value. It is somewhat surprising that sites which are coupled through the network, though not directly, yield zero for the integral—this suggests that there is a hidden topological property in the frequency-dependent two-point measurement between non-directly-connected sites.

The power of this approach is clear: even with a tremendous number of modes (approaching a continuum), the bare frequency of a single resonator, or the tunnel coupling between a pair of resonators, can be directly extracted from one- or two-port frequency-dependent measurements. This provides a robust linear method for estimating matrix elements of the Hamiltonian that is much less sensitive to noise than other methods involving, e.g., fitting of all coupled modes. Handling the logarithmic divergence of the integral (formally taken care of via a Cauchy principal value) requires some care, however, and we suggest two approaches as follows.

(1) In small lattices, where the individual normal modes are spectrally resolved, the integrals may be performed by identifying and fitting the individual resonances in the one- or two-port measurements, and then evaluating the integrals as sums over said resonances [here  $A_l^{\alpha\beta}$ ,  $\phi_l^{\alpha\beta}$ ,  $\omega_l^{\alpha\beta}$ ,  $\gamma_l^{\alpha\beta}$  are the parameters resulting from the fit to the observed (offset-corrected) two-point spectrum between sites  $\alpha$  and  $\beta$ ,  $S_{\alpha\beta}^{\text{obs}}(\omega)$ ]:

$$\begin{aligned}
S_{\alpha\beta}^{\text{obs}}(\omega) &= \sum_l \frac{A_l^{\alpha\beta} e^{i\phi_l^{\alpha\beta}}}{1 + i \frac{(\omega - \omega_l^{\alpha\beta})}{\gamma_l^{\alpha\beta}/2}}, \\
\mathbf{N}^\alpha &\equiv \int S_{\alpha\alpha}^{\text{obs}}(\omega) d\omega \\
&= \frac{\pi}{2} \sum_l A_l^{\alpha\alpha} e^{i\phi_l^{\alpha\alpha}} \gamma_l^{\alpha\alpha}, \\
\mathbf{X}^{\alpha\beta} &\equiv \int \omega S_{\alpha\beta}^{\text{obs}}(\omega) d\omega - \frac{W \langle \alpha | \beta \rangle}{i\pi} \sqrt{\mathbf{N}^\alpha \mathbf{N}^\beta} \\
&= \frac{\pi}{2} \sum_l A_l^{\alpha\beta} e^{i\phi_l^{\alpha\beta}} \gamma_l^{\alpha\beta} (\omega_l^{\alpha\beta} + i\gamma_l^{\alpha\beta}/2), \\
\langle \alpha | H | \beta \rangle &= \frac{\mathbf{X}^{\alpha\beta}}{\sqrt{\mathbf{N}^\alpha \mathbf{N}^\beta}}. \tag{5}
\end{aligned}$$

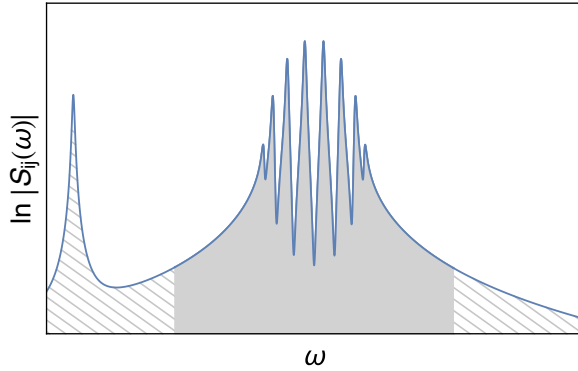


FIG. 1. Truncation of integration region. To avoid the divergence in the integration of the tails of the transmission and reflection spectra, the symmetric tails of the spectra should be identified by the locations in the spectra where the lattice response has reduced to a simple Lorentzian, decaying as  $1/\Delta$  (for  $S_{\alpha\alpha}$ , the decay is  $1/\Delta^2$ ; for  $S_{\alpha\beta}$ ,  $\alpha \neq \beta$ ), and their values are identical. Here  $\Delta$  is the detuning of the probe frequency to the manifold of resonances being considered. The integration then should only be performed between these two points (area in gray), and the divergence of the tails (area in gray stripes) will then cancel. In practice, choosing the cutoff location is a trade-off between ensuring that one is far enough from the resonant features to be in regions with  $1/\Delta$  (or  $1/\Delta^2$ ) decay, but not so far out that other resonator modes (corresponding to parasitic resonances outside of the effective model as shown at the left, or other bands within the effective model) become important. The impact of these other modes on the integration can be further reduced using the technique outlined in Appendix A.

(2) In larger lattices, where the individual modes cannot be spectrally resolved, the integrals may be explicitly computed from the observed spectra, taking care to symmetrically cut off the tails at low and high frequencies, to cancel the logarithmic divergence of the integration (see Fig. 1). Note that this cutoff need not be perfect, especially for the normalization terms (coming from reflection measurements), where the divergence is logarithmic. On the other hand, the integration in Eq. (4) diverges linearly for on-site matrix elements ( $\alpha = \beta$ ) of the Hamiltonian, so it is crucial to subtract off the integration-range dependent correction given by the second term.

In both cases, it is assumed that  $\mathbf{N}^{\alpha,\beta}$  are real; errors from finite integration region and imperfect centering could render them complex, and so we assume that the imaginary part of the integration is simply discarded (see Appendix C). On the other hand,  $\mathbf{X}^{\alpha\beta}$  are assumed complex: for  $X^{\alpha\alpha}$ , the real part arises from the on-site energy, and the imaginary part from on-site loss; for complex  $X^{\alpha\beta}$  with  $\beta \neq \alpha$ , this corresponds to either a phase on the tunneling term if  $X^{\alpha\beta} = (X^{\beta\alpha})^*$ , or lossy tunneling if  $X^{\alpha\beta} = -(X^{\beta\alpha})^*$ , and a general term may be decomposed into a combination of the two.

Note also that low-area peaks contribute in proportion to their area to the value of measured Hamiltonian matrix element, so finite signal-to-noise ratio is likely not a fundamentally limiting factor in the same way that it would be if one attempted to use many transmission and reflection measurements to fully invert and extract the lattice Hamiltonian; missing a small peak makes inverting the Hamiltonian fundamentally impossible, while it produces errors in spectroscopy of a

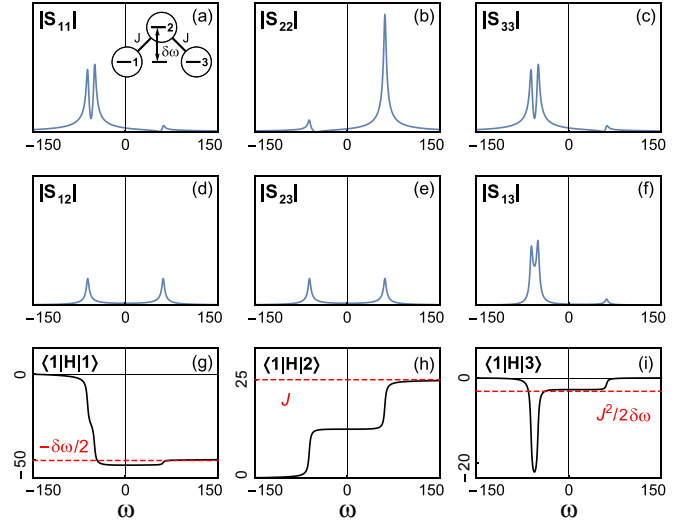


FIG. 2. Three site spectroscopy. (a)–(c) Reflection spectra of sites 1, 2, and 3, respectively, of a three-site tight-binding chain, whose outer sites are at equal energies, while the central site is detuned [(a), inset]. (d)–(f) Transmission spectra for 1-2, 2-3, and 1-3, respectively. All spectra are plotted as the absolute value of the amplitude, and share a common (arbitrary) normalization. The spectra exhibit a low-energy doublet resulting from second-order coupling between sites 1 and 3, and an isolated high-energy peak arising from the central site. (g)–(i) Application of the Hamiltonian estimation technique of Eq. (4) to the three-site chain, as a function of the numerical integration range. We fix the lower limit of integration at  $-150$  MHz and vary the upper limit between  $-150$  MHz and  $150$  MHz. (g) On-site energy of site 1, converging to within  $J^2/\delta\omega$  of  $-\delta\omega/2$  once the integration range includes the doublet, and the rest of the way once the high-energy feature is included. (h) The tunneling matrix element between sites 1 and 2, converging only once all spectral features are included. (i) The tunneling matrix element between sites 1 and 3, which is zero in our model. For (g)–(i) we plot only the real part of the estimated matrix elements, as the imaginary part converges less rapidly.

particular matrix element on the order of that peak's fractional area.

Particular care must be taken in the calibration of phases in spectroscopy: Any physical coupler will likely introduce additional frequency dependent phase variations to the spectra, arising from the structure of the coupler itself. This prohibits a high-accuracy calibration of the  $\kappa_c$ 's, which would necessitate detuning a single cavity from its neighbors, or removing the tunnel couplers to its neighbors, so that the cavity's frequency and linewidth are directly observable as a single resonance peak. The phase variation can then be obtained from the measured reflection spectrum, and subsequently used to calibrate all other spectra.

As a simple demonstration of this technique, we consider a three-site tight-binding model, as shown in Fig. 2(a), inset, where the outer two sites are tuned to frequency  $\omega_0 - \delta\omega/2$ , and the central site is tuned to frequency  $\omega_0 + \delta\omega/2$ ; the outer two sites are coupled to the central site with a tunneling energy  $J$ . Figures 2(a)–2(f) show computed reflection and transmission spectra  $S_{11}$ ,  $S_{22}$ ,  $S_{33}$ ,  $S_{12}$ ,  $S_{23}$ , and  $S_{13}$ , respectively. As expected the outer two sites hybridize through an

effective second-neighbor coupling  $\sim J^2/\delta\omega$ , while the central site's resonance is detuned by  $\sim\delta\omega$ . For  $\delta\omega = 100$  MHz,  $J = 25$  MHz, Fig. 2(g) shows the on-site energy  $\langle 1|H|1\rangle$  extracted via the tomography technique from the preceding section, as the upper limit of integration is varied. It is apparent that the site-energy converges to within  $\sim J^2/\delta\omega$  of the correct value as soon as the integration region includes the low-energy doublet, and is further corrected as the region passes across the isolated (and small) high-energy resonance. To extract  $\langle 1|H|2\rangle$ , Fig. 2(h) shows the tomography result as a function of the upper limit of integration; once all resonances are included, this value converges to  $J$ , as anticipated. Finally, Fig. 2(i) shows the tunneling matrix element  $\langle 1|H|3\rangle$  as a function of the upper limit of the integration; for a range that only includes the doublet, the tomography procedure yields a result proportional to the second-order tunneling rate of  $J^2/\delta\omega$  (though this precise value is not obtained: the probed lattice sites are not the ‘‘Wannier functions’’ of the effective theory once the central site has been adiabatically eliminated, and thus there are corrections; see Appendix A); once the high-energy resonance is included, the true tunneling rate of zero is recovered.

### B. Band projectors and real-space measurement of the Chern number

An emerging goal in synthetic topological materials is to characterize their topological invariants. While the Hall conductivity is the method of choice in solid state, transport measurements can be challenging in synthetic systems, particularly those where the ‘‘charge carriers’’ are bosons rather than fermions. Furthermore, such systems are typically subject to both disorder effects, and the impact of finite size and boundaries, both of which break the translational invariance necessary for application of the TKNN formula [27] for the Chern invariant. In a seminal work [28], Kitaev proved that the Chern number could be computed for a disordered system, so long as the disorder is small enough that the bands remain spectrally isolated from one another. In this case, one may define a projector into band  $\mu$  with matrix elements between lattice sites  $\alpha$  and  $\beta$ :

$$P_{\alpha\beta}^{\mu} \equiv \langle \alpha | \left[ \sum_{n \in \text{band } \mu} |n\rangle \langle n| \right] | \beta \rangle. \quad (6)$$

If the sites in the bulk of the system are then partitioned into three nonoverlapping but adjacent regions  $A, B, C$ , as in Fig. 3, the Chern number may be written:

$$C^{\mu} = 12\pi i \sum_{\alpha \in A, \beta \in B, \gamma \in C} (P_{\alpha\beta}^{\mu} P_{\beta\gamma}^{\mu} P_{\gamma\alpha}^{\mu} - P_{\alpha\gamma}^{\mu} P_{\gamma\beta}^{\mu} P_{\beta\alpha}^{\mu}). \quad (7)$$

While the regions  $A$ ,  $B$ , and  $C$  must be infinitely large to ensure precise convergence of the Chern number to the TKNN invariant defined from the band structure, in practice a region which is several unit cells (or equivalently magnetic unit cells, in the case of the Hofstadter model) is sufficient to achieve reasonable convergence (at the  $\sim 99\%$  level; see Fig. 4(a)). Furthermore, it is essential that  $A$ ,  $B$ , and  $C$  avoid the system edges, as these provide a contribution to  $C_{\mu}$  which precisely

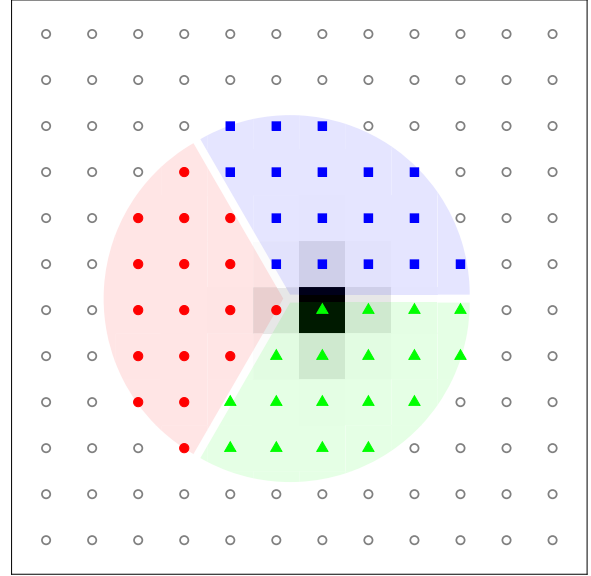


FIG. 3. Measuring Chern numbers in real space. To measure the Chern number of a disordered band in the bulk of a Chern insulator, a bulk region large compared to the unit cell size (magnetic length in the Hofstadter model, whose band projector onto an arbitrary bulk site is shown as gray-scale squares for  $\alpha = \frac{1}{4}$ ) is partitioned into three similarly sized regions (red circles, green triangles, and blue squares). The difference of triple band-projector products red  $\rightarrow$  green  $\rightarrow$  blue and blue  $\rightarrow$  green  $\rightarrow$  red, summed over all sites in each region, is equal to the Chern number  $C/(12\pi i)$ . There are a number of ways to spectroscopically measure this projector, discussed in the text.

cancels that of the bulk. This approach may be understood as a direct measurement of the nonreciprocity of the system, as it compares  $A \rightarrow B \rightarrow C$  coupling to  $C \rightarrow B \rightarrow A$  coupling, similar to the case in a Faraday isolator [29]. As shown in Fig. 4(b), as long as the disorder is an order of magnitude smaller than the band spacing, Chern number quantization is preserved.

The challenge then is to measure the band projector using the spectroscopic tools at our disposal. We suggest three approaches as follows.

- (1) Consider the integral

$$\begin{aligned} M_{\alpha\beta}^{\mu} &\equiv \text{Pr} \left[ \frac{i}{\sqrt{\kappa_c^{\alpha} \kappa_c^{\beta}}} \int_{\omega \in \text{band } \mu} d\omega S_{\alpha\beta}(\omega) \right] \\ &= \text{Pr} \left[ \int d\omega \langle \alpha | \frac{1}{\omega - H} | \beta \rangle \right] \\ &= \text{Pr} \left[ \int d\omega \sum_n \frac{\langle \alpha | n \rangle \langle n | \beta \rangle}{\omega - \epsilon_n} \right]. \end{aligned}$$

Assuming good band flatness  $\frac{\text{bandwidth}}{\text{band spacing}} \ll 1$  [30,31], we can integrate across band  $\mu$  without accruing a substantial contribution from the other bands, yielding  $M_{\alpha\beta}^{\mu} \approx i\pi \langle \alpha | [\sum_{n \in \text{band } \mu} |n\rangle \langle n|] | \beta \rangle$ . Therefore,  $P_{\alpha\beta}^{\mu} \approx$

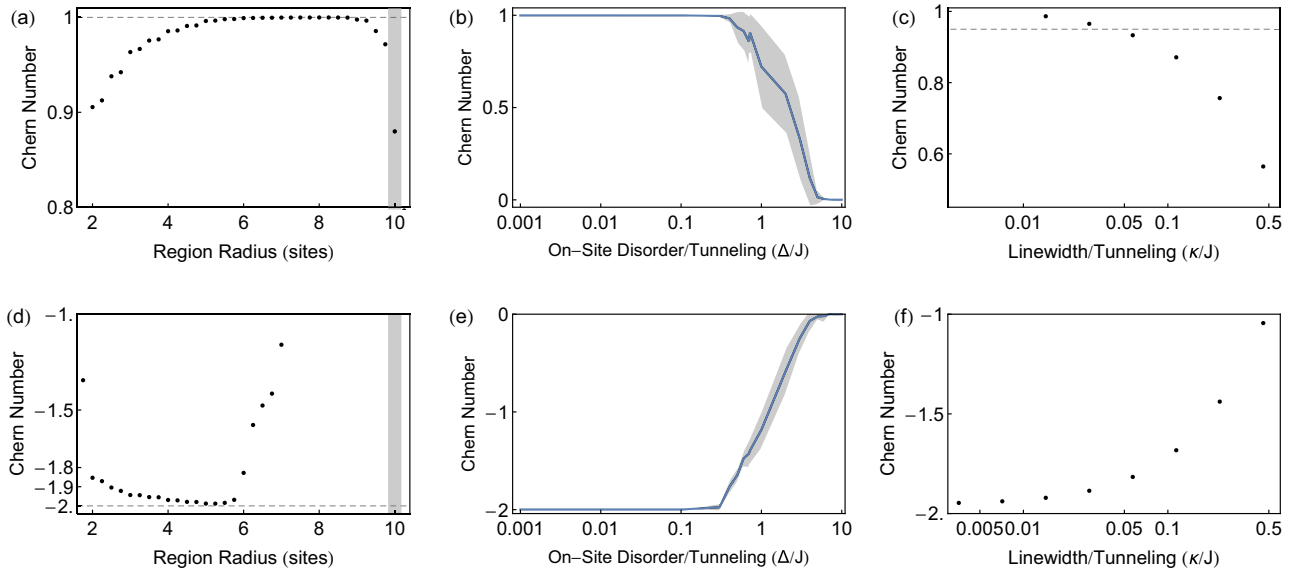


FIG. 4. Technical limitations of Chern number measurement. (a) Numerically computed dependence of the spectroscopically extracted Chern number of the lowest band upon region radius for an array of lossless resonators coupled in an  $\alpha = \frac{1}{4}$  Hofstadter configuration. Once the radius exceeds a magnetic length ( $\frac{1}{\alpha} = 4$  sites), the measured value approaches the translationally invariant TKNN value  $C = 1$ ; it drops at the system edge (gray bar). (b) Numerically computed Chern number vs the rms variation in on-site energy. The error band shows the variation over disorder realizations; the Chern number is robust to disorder up to  $\sim 0.1 \times J$ , comparable to the band splitting of the model. (c) Numerically computed Chern number vs resonator linewidth (in units of tunneling energy), using a frequency integration of the two port measurement  $S_{\alpha\beta}(\omega)$ , as described in the text, for a region with five site radius. A loss rate  $\leq 0.03 \times$  tunneling provides a fidelity  $\geq 0.95$ . (d)–(f) Identical calculations for the two middle bands of the  $\alpha = \frac{1}{4}$  Hofstadter lattice, which touch at Dirac points and thus must be analyzed together. The extracted Chern number  $C = -2$  is consistent with the TKNN formula.

$\frac{1}{i\pi} M_{\alpha\beta}^{\mu}$ . It is thus sufficient to integrate the properly normalized  $S_{\alpha\beta}(\omega)$  over a single energy band  $\mu$  to extract the matrix element of the projector onto band  $\mu$  between sites  $\alpha$  and  $\beta$ . This integral is only logarithmically sensitive to the limits of integration, so precise cancellation of the tail contributions from finite linewidth and imperfect flatness are possible at near unity fidelities.

(2) Consider a continuous-wave excitation at site  $\beta$  within the bulk of the lattice, at an energy  $\hbar\omega_o$  detuned from band  $\mu$  by an amount large compared to its width, but small compared with its detuning to other bands. Generically, response at site  $\alpha$  is given by  $S_{\alpha\beta}(\omega_o) = -i\sqrt{\kappa_c^{\alpha}\kappa_c^{\beta}} \sum_n \frac{\langle\alpha|n\rangle\langle n|\beta\rangle}{\omega_o - \epsilon_n}$ . Imposing that the detuning to all other bands is large, their contribution may be discarded. If we can simultaneously assume that  $\omega_o - \epsilon_n = \Delta_n$  is approximately constant for all  $n$  in band  $\mu$ ,  $\Delta_n = \Delta$ , then we have  $S_{\alpha\beta}(\omega_o) \approx -\frac{i\sqrt{\kappa_c^{\alpha}\kappa_c^{\beta}}}{\Delta} \sum_{n \in \text{band } \mu} \langle\alpha|n\rangle\langle n|\beta\rangle$ , and thus  $P_{\alpha\beta}^{\mu} \approx \frac{i\Delta}{\sqrt{\kappa_c^{\alpha}\kappa_c^{\beta}}} S_{\alpha\beta}(\omega_o)$ .

(3) Consider an excitation pulse at site  $\beta$  within the bulk of the lattice, with a well-defined carrier frequency centered on band  $\mu$ , and temporally short wave packet (Gaussian, for maximum spectral efficiency). If this pulse is sufficiently short in time to provide a spectral bandwidth larger than band  $\mu$ , while simultaneously long enough to not excite other bands, the transmitted response of the system at site  $\alpha$  immediately after the pulse will reflect the matrix element of the projector into band  $\mu$  between sites  $\alpha$  and  $\beta$ . If the pulse is too spectrally narrow compared with the bandwidth of band  $\mu$ , the excitation

will evolve spatially before the pulse has terminated, and the projector cannot be extracted.

The second and third approaches impose much more stringent requirements on the band flatness than the first, and as such will not work well for Hofstadter models at high flux per plaquette.

In any of these approaches, it should be possible, in the low-disorder limit, to make use of the approximate translational invariance from one magnetic unit cell to the next to reduce the number of measurements from  $\sim N^2$ , where  $N$  is the number of sites in one of the regions  $A, B, C$ , to  $\sim q \times N$ , where  $q$  is the number of sites within the magnetic unit cell (equal to 4 for an  $\alpha = \frac{1}{4}$  Hofstadter lattice). Because  $N \sim q^2$ , the total number of two-point spectra required to extract the Chern number is thus  $\sim q^3$ .

A more fundamental limit comes from the finite lifetime of a photon in the lattice (due to absorption, for example), which may cause the photon to be lost before it can explore enough of the lattice to provide a stable Chern number  $C_{\mu}$ . As shown in Fig. 4(c), the Chern number can be measured with fidelity above 95% so long as the tunneling rate is 30 $\times$  the photon decay rate, for the lowest band of an  $\alpha = \frac{1}{4}$  Hofstadter model, in spite of the substantial band curvature. The requirement on tunneling compared to decay is consistent with the particle needing time to explore an area whose radius is the magnetic length  $\sim q$ , to be sensitive to the Chern number. Further, Figs. 4(d)–4(f) demonstrate that this technique is capable of extracting negative Chern numbers, as well as Chern numbers with magnitude larger than one.

### III. OUTLOOK

We have provided a tool set for characterizing photonic lattices using one- and two- point measurements to resolve matrix elements of the Hamiltonian. We have further introduced a recipe to extract the band projector, allowing direct measurement of Chern number in real space. While the proposed approach is designed for photonic lattices where network analyzer technology is commercially available, it can be applied much more broadly (see Appendix D) to explore properties of optical resonators [32] and resonator arrays [33], coupled quantum dots, mechanical and acoustical systems [34–38], and potentially even electronic systems by reinterpreting STM measurements. It should further be possible to measure Chern invariants of the energy “bands” of topological quasiperiodic structures [39], where extremely low-loss materials and large measurement areas will be necessary to overcome the small band gaps and large quasicrystalline unit cells.

### ACKNOWLEDGMENTS

We would like to thank Brandon Anderson, William Irvine, Charles Kane, Michael Levin, Nathan Schine, and Norman Yao for fruitful discussions. This work was supported by ARO Grant No. W911NF-15-1-0397. D.I.S. acknowledges support from the David and Lucile Packard Foundation; R.M. acknowledges support from the University of Chicago MRSEC program of the NSF under Grant No. NSF-DMR-MRSEC 1420709; C.O. is supported by the NSF GRFP.

### APPENDIX A: COUPLING TO MULTIPLE SITES

In practice, one must be careful to avoid accidental *direct* coupling to multiple lattice sites when performing the spectroscopy of a tunnel-coupled lattice system. Such direct couplings arise naturally because in any real lattice the Wannier functions are not perfectly localized to individual lattice sites. This nonlocal tail means while the in and out couplers are physically connected only to individual sites, they will drive and measure multiple lattice sites.

To understand the consequences of this, consider two degenerate sites at energy  $\omega_0$ ,  $|a\rangle$  and  $|b\rangle$ , that are tunnel coupled with an energy  $J$ , such that the Hamiltonian in the one-excitation manifold is  $H_0 = \omega_0(|a\rangle\langle a| + |b\rangle\langle b|) - J(|a\rangle\langle b| + |b\rangle\langle a|)$ . Now we drive with a coupler  $|\mu\rangle \equiv \cos \epsilon|a\rangle + \sin \epsilon|b\rangle$  (predominantly connected to site  $a$ ), and measure with coupler  $|\nu\rangle \equiv \cos \epsilon|b\rangle + \sin \epsilon|a\rangle$  (predominantly connected to site  $b$ ), corresponding to a Wannier overlap of  $\sim \epsilon^2$  on adjacent sites.

We then measure  $S_{\mu\mu}(\omega)$ ,  $S_{\nu\nu}(\omega)$ , and  $S_{\mu\nu}(\omega)$ , and attempt to extract the Hamiltonian matrix elements. Applying the spectroscopy techniques from the text yields  $\langle \mu|H_0|\mu\rangle_{\text{Spec}} = \langle \nu|H_0|\nu\rangle_{\text{Spec}} = \omega_0 - J \sin 2\epsilon$  and  $\langle \mu|H_0|\nu\rangle_{\text{Spec}} = -J + (\omega_0 - iW/\pi) \sin 2\epsilon$ . We anticipated that  $S_{\mu\mu}(\omega)$  and  $S_{\nu\nu}(\omega)$  would provide on-site energies, while  $S_{\mu\nu}(\omega)$  was to provide the tunneling energy. In reality, we find that the on-site energy experiences a small correction from the tunneling energy, which, in the tight-binding limit (where  $\epsilon \ll 1$ ), is almost certainly negligible. By contrast, the error in the tunneling energy may be *much* larger than  $J$  itself if  $\epsilon \geq \frac{J}{\omega_0}$ .

To circumvent this systematic issue, the measurements of  $\langle \alpha|H|\beta\rangle$  may be reorthogonalized using a basis transformation based upon the matrix  $\int d\omega S_{\alpha\beta}(\omega)$ . A simpler solution is to shift all frequencies by some constant  $\Omega \sim \omega_0$ , and then employ  $\tilde{S}_{\mu\nu}(\omega) = S_{\mu\nu}(\omega - \Omega)$  for all resolvent calculations. We are then measuring matrix elements of  $H_0 - \mathbb{1}\Omega$ , and thus the error in the measurement of  $J$  will be of order  $(\omega_0 - \Omega) \sin \epsilon \leq J \sin \epsilon$ , and thus small.

### APPENDIX B: BRUTE-FORCE INVERSION OF A 1D CHAIN THROUGH A REFLECTION MEASUREMENT

Here we summarize an existing brute-force approach [12] to extracting the properties of a 1D tight-binding chain, using only reflection measurements off of its end. This should be compared with the approach put forth in this work, which extracts a single Hamiltonian matrix element from each measured spectrum, but with superior numerical stability.

Consider a 1D chain characterized entirely by nearest-neighbor tunneling matrix elements  $t_\mu$  between sites  $\mu$  and  $\mu + 1$ , and on-site energy of site  $\mu$ ,  $\delta_\mu$ :

$$H_{1D} = \sum_{\mu} [\delta_{\mu} a_{\mu}^{\dagger} a_{\mu} - (t_{\mu} a_{\mu+1}^{\dagger} a_{\mu} + t_{\mu}^{*} a_{\mu}^{\dagger} a_{\mu+1})]. \quad (\text{B1})$$

For  $n$  lattice sites, this system has  $2n - 1$  unknowns, coming from the  $n$  on-site energies, and  $n - 1$  tunneling matrix elements; it is thus conceivable that measuring the  $n$  eigenmode energies, and  $n$  spectral weights (the latter providing  $n - 1$  linearly independent pieces of information, due to normalization), via a reflection measurement off of a single lattice site, would be enough to extract all system parameters. Symmetry precludes this unless the probed site is at the end of the 1D chain, as proven previously in Burgarth *et al.* [12].

The prescription we summarize [12] allows extraction of all on-site energies  $\delta_\mu$  and tunneling matrix elements  $t_\mu$ , from measured resonance frequencies  $\omega^j$  and their spectral weights  $\psi_{\mu=0}^j$ , normalized such that  $\sum_j |\psi_{\mu=0}^j|^2 = 1$ . With measurements only at one end of the chain ( $\mu = 0$ ), we obtain all relevant lattice parameters:

$$\begin{aligned} \delta_{\mu} &= \sum_j \omega^j |\psi_{\mu-1}^j|^2, \\ |t_{\mu}| &= \sqrt{\sum_j [(\omega^j - \delta_{\mu}) \psi_{\mu-1}^j - |t_{\mu-1}| \psi_{\mu-2}^j]^2}, \\ \psi_{\mu}^j &= \frac{1}{|t_{\mu}|} [\psi_{\mu-1}^j (\omega^j - \delta_{\mu}) - |t_{\mu-1}| \psi_{\mu-2}^j]. \end{aligned} \quad (\text{B2})$$

Here we have implicitly assumed  $\psi_{\mu=-1}^j = 0$  for all  $j$ . Raised, Roman indices refer to eigenmodes, while lowered, Greek indices refer to sites, counted from the probed end of the chain. Note that the expression for  $\delta_{\mu=0}$  reduces to the results from the main text.

### APPENDIX C: EXTRACTING COUPLING STRENGTH

In this appendix we derive the following relation, employed in the text:  $\int S_{\alpha\alpha}(\omega) d\omega = \pi \kappa_c^{\alpha}$ ; we follow the procedure used

in the text to derive a related expression for  $\int \omega S_{\alpha\beta}(\omega)d\omega$ ,

$$\begin{aligned}
\int S_{\alpha\alpha}(\omega)d\omega &= -i\kappa_c^\alpha \int \langle \alpha | \frac{1}{\omega - H} | \alpha \rangle d\omega \\
&= -i\kappa_c^\alpha \int \langle \alpha | \sum_{\mu} \frac{|\mu\rangle\langle\mu|}{\omega - \epsilon_{\mu}} | \alpha \rangle d\omega \\
&= -i\kappa_c^\alpha \langle \alpha | \sum_{\mu} \left[ \int \frac{|\mu\rangle\langle\mu|}{\omega - \epsilon_{\mu}} d\omega \right] | \alpha \rangle \\
&= -i\kappa_c^\alpha \langle \alpha | \alpha \rangle \arctan x \Big|_{-\infty}^{+\infty} \\
&= \pi \kappa_c^\alpha. \tag{C1}
\end{aligned}$$

To quantify the impact of finite integration region and imperfect centering of said region on the resonances, we evaluate the arc tangent over an interval of integration  $[\omega_0 - \Omega - \delta, \omega_0 + \Omega - \delta]$ , where  $\omega_0$  is the center frequency of a particular resonance,  $2\Omega$  is the width of the integration region, and  $\delta$  is the centering error. This leads to a result of  $\pi \kappa_c^\alpha (1 + \frac{\Gamma}{\pi\Omega} - i \frac{2\delta}{\pi\Omega})$ , where  $\Gamma$  is the width of the resonance under consideration. In short, centering errors do not impact the value of  $\kappa_c^\alpha$  at lowest order, so long as the imaginary part of the  $\kappa_c^\alpha$  extracted from this calculation is simply discarded.

#### APPENDIX D: POTENTIAL EXPERIMENTAL APPLICATIONS

Our technique is applicable to a wide array of experimental platforms; here we briefly explore the benefits and difficulties inherent to each.

##### 1. Microwave resonator arrays

An array of tunnel-coupled microwave resonators provide a near-ideal realization of the models that we would like to tomographically characterize using the techniques developed in this work. These resonator arrays have now been demonstrated in the strongly interacting [40] and ultralow disorder [10] regimes, though not yet both simultaneously; furthermore, there are proposals [41] and, recently, demonstrations [42] of tight-binding microwave Chern insulators in resonator arrays.

The strength of microwave resonator arrays is the ability to individually address the chosen lattice sites by simply moving the probes [43]; this affords spatially and energetically (or temporally) localized measurement of lattice properties. Proper phase and amplitude calibration of the network analyzer permits complete reconstruction of the complex two-site transfer function.

The primary challenge faced in microwave setups is that the Wannier orbitals (defining the tight-binding basis) may not be entirely localized to individual lattice sites, and so site-localized probes are likely to couple in a complicated way to the tight-binding sites. This effect may be quantified by

noting that, in the tight-binding basis,  $\int_{\text{all bands}} S_{\alpha\beta}(\omega)d\omega = \delta_{\alpha\beta}$ ; off-diagonal contributions indicate nonlocal Wannier wave functions.

##### 2. Mechanical resonator arrays

Recent experiments with arrays of coupled mechanical oscillators [34–38] suggest another platform where our approach could be employed. The ability to locally drive the systems and, in most cases, measure the response at all sites using real-time video, makes extraction of  $S_{\alpha\beta}(\omega)$  straightforward.

A challenge is that these systems often do not have much separation between positive- and negative- energy eigenmodes, in units of their tunnel coupling ( $J \sim \omega_0$ ); this means that a tight-binding model is often a far-from-ideal description of the dynamics in the system, and the basic approach of this work breaks down. Furthermore, the relatively low quality factor of the mechanical oscillators employed means that excitations do not typically propagate very far within their lifetimes, limiting efficacy of the band-projector and Chern-number measurement prescriptions. On a practical note, the extraordinarily long time scales of such experiments ( $\geq 1$  s to reach steady state [35]) means that the time required to site- and energy- resolved spectroscopy could be prohibitive.

##### 3. Near degenerate multimode optical resonators

The many transverse modes of an optical resonator (for a fixed longitudinal mode number) provide a Floquet-like implementation of a 2D quadratic Hamiltonian [44]. This analogy is quite familiar from studies of exciton polariton condensates [45] and photonic BECs [46], but has recently been harnessed to generate Landau levels for optical photons [32]. Typical resonator finesses of  $\geq 10^4$  allow for many classical cyclotron orbits within the particle lifetime.

While this is a continuum system, the Chern number formula still applies to its Landau levels, so long as the spacing between “sample points” (akin to lattice sites in the periodic system) is small compared with the magnetic length. The ability to image the *entire* transmitted resonator field on a CCD, combined with broadband tunability of the probing laser and availability of spatial light modulators to inject light at an arbitrary position, will make measurement of band projectors (in this case, Landau-level projectors) straightforward. The challenge will be extraction of the phase of the transmitted optical field, which we propose to do by interfering the transmitted resonator field with a reference light field, and using the interference pattern to holographically reconstruct the phase of the projector.

Another potential complication is that the mirror transmission itself may vary spatially, akin to a site-dependent  $\kappa_c^\alpha$  in the language of the paper. This will then need to be independently calibrated either directly (with a uniform laser beam incident on the out-coupling mirror) or using a technique akin to Eq. (5).

[1] G.-B. Jo, J. Guzman, C. K. Thomas, P. Hosur, A. Vishwanath, and D. M. Stamper-Kurn, *Phys. Rev. Lett.* **108**, 045305 (2012).  
[2] L. Tarruell, D. Greif, T. Uehlinger, G. Jotzu, and T. Esslinger, *Nature (London)* **483**, 302 (2012).

[3] M. Greiner, O. Mandel, T. Esslinger, T. W. Hansch, and I. Bloch, *Nature (London)* **415**, 39 (2002).  
[4] K. K. Gomes, W. Mar, W. Ko, F. Guinea, and H. C. Manoharan, *Nature (London)* **483**, 306 (2012).

- [5] A. González-Tudela, C.-L. Hung, D. Chang, J. Cirac, and H. Kimble, *Nat. Photon.* **9**, 320 (2015).
- [6] W. S. Bakr, J. I. Gillen, A. Peng, S. Fölling, and M. Greiner, *Nature (London)* **462**, 74 (2009).
- [7] T. Gericke, P. Würtz, D. Reitz, T. Langen, and H. Ott, *Nat. Phys.* **4**, 949 (2008).
- [8] D. Husmann, S. Uchino, S. Krinner, M. Lebrat, T. Giamarchi, T. Esslinger, and J.-P. Brantut, *Science* **350**, 1498 (2015).
- [9] W. S. Bakr, A. Peng, M. E. Tai, R. Ma, J. Simon, J. I. Gillen, S. Fölling, L. Pollet, and M. Greiner, *Science* **329**, 547 (2010).
- [10] D. L. Underwood, W. E. Shanks, J. Koch, and A. A. Houck, *Phys. Rev. A* **86**, 023837 (2012).
- [11] H. L. Stormer, D. C. Tsui, and A. C. Gossard, *Rev. Mod. Phys.* **71**, S298 (1999).
- [12] D. Burgarth, K. Maruyama, and F. Nori, *Phys. Rev. A* **79**, 020305(R) (2009).
- [13] D. Burgarth and K. Maruyama, *New J. Phys.* **11**, 103019 (2009).
- [14] K. Takayanagi, *Nucl. Phys. A* **510**, 162 (1990).
- [15] C.-E. Bardyn, S. D. Huber, and O. Zeitler, *New J. Phys.* **16**, 123013 (2014).
- [16] M. Hafezi, *Phys. Rev. Lett.* **112**, 210405 (2014).
- [17] T. Ozawa and I. Carusotto, *Phys. Rev. Lett.* **112**, 133902 (2014).
- [18] C. Cohen-Tannoudji, J. Dupont-Roc, and G. Grynberg, *Atom-photon Interactions: Basic Processes and Applications* (Wiley, New York, 1992).
- [19] I. Rotter, *J. Phys. A* **42**, 153001 (2009).
- [20] A. Sommer, H. P. Büchler, and J. Simon, [arXiv:1506.00341](https://arxiv.org/abs/1506.00341).
- [21] H. A. Weidenmüller, *Ann. Phys. (NY)* **158**, 120 (1984).
- [22] M. C. Zheng, in Master's Thesis, Wesleyan University, 2009.
- [23] M. O. Scully and M. S. Zubairy, *Quantum Optics* (Cambridge University Press, Cambridge, 1997).
- [24] A. Wallraff, D. I. Schuster, A. Blais, L. Frunzio, R.-S. Huang, J. Majer, S. Kumar, S. M. Girvin, and R. J. Schoelkopf, *Nature (London)* **431**, 162 (2004).
- [25] J. Ningyuan, C. Owens, A. Sommer, D. Schuster, and J. Simon, *Phys. Rev. X* **5**, 021031 (2015).
- [26] V. V. Albert, L. I. Glazman, and L. Jiang, *Phys. Rev. Lett.* **114**, 173902 (2015).
- [27] D. J. Thouless, M. Kohmoto, M. P. Nightingale, and M. den Nijs, *Phys. Rev. Lett.* **49**, 405 (1982).
- [28] A. Kitaev, *Ann. Phys. (NY)* **321**, 2 (2006).
- [29] C. L. Hogan, *Rev. Mod. Phys.* **25**, 253 (1953).
- [30] T. Neupert, L. Santos, C. Chamon, and C. Mudry, *Phys. Rev. Lett.* **106**, 236804 (2011).
- [31] N. Y. Yao, C. R. Laumann, A. V. Gorshkov, S. D. Bennett, E. Demler, P. Zoller, and M. D. Lukin, *Phys. Rev. Lett.* **109**, 266804 (2012).
- [32] N. Schine, A. Ryou, A. Gromov, A. Sommer, and J. Simon, *Nature (London)* **534**, 671 (2016).
- [33] M. Hafezi, S. Mittal, J. Fan, A. Migdall, and J. Taylor, *Nat. Photon.* **7**, 1001 (2013).
- [34] L. M. Nash, D. Kleckner, A. Read, V. Vitelli, A. M. Turner, and W. T. Irvine, *Proc. Natl. Acad. Sci. USA* **112**, 14495 (2015).
- [35] R. Süsstrunk and S. D. Huber, *Science* **349**, 47 (2015).
- [36] J. A. Franco-Villafañe, E. Sadurní, S. Barkhofen, U. Kuhl, F. Mortessagne, and T. H. Seligman, *Phys. Rev. Lett.* **111**, 170405 (2013).
- [37] M. Bellec, U. Kuhl, G. Montambaux, and F. Mortessagne, *Phys. Rev. B* **88**, 115437 (2013).
- [38] A. Morales, J. Flores, L. Gutiérrez, and R. Méndez-Sánchez, *J. Acoust. Soc. Am.* **112**, 1961 (2002).
- [39] M. A. Bandres, M. C. Rechtsman, and M. Segev, *Phys. Rev. X* **6**, 011016 (2016).
- [40] M. Fitzpatrick, N. M. Sundaesan, A. C. Y. Li, J. Koch, and A. A. Houck, *Phys. Rev. X* **7**, 011016 (2017).
- [41] B. M. Anderson, R. Ma, C. Owens, D. I. Schuster, and J. Simon, *Phys. Rev. X* **6**, 041043 (2016).
- [42] P. Roushan, C. Neill, A. Megrant, Y. Chen, R. Babbush, R. Barends, B. Campbell, Z. Chen, B. Chiaro, A. Dunsworth *et al.*, *Nat. Phys.* **13**, 146 (2017).
- [43] D. L. Underwood, W. E. Shanks, A. C. Y. Li, L. Ateshian, J. Koch, and A. A. Houck, *Phys. Rev. X* **6**, 021044 (2016).
- [44] A. Sommer and J. Simon, *New J. Phys.* **18**, 035008 (2016).
- [45] J. Kasprzak, M. Richard, S. Kundermann, A. Baas, P. Jeambrun, J. Keeling, F. Marchetti, M. Szymańska, R. Andre, J. Staehli *et al.*, *Nature (London)* **443**, 409 (2006).
- [46] J. Klaers, J. Schmitt, F. Vewinger, and M. Weitz, *Nature (London)* **468**, 545 (2010).